International Journal of Physical Research, 14 (1) (2026) 9-20

International Journal of Physical Research

Website: www.sciencepubco.com/index.php/IJPR
https://doi.org/10.14419/24s4as93
Research paper

Determination of Basement Depth Using Aeromagnetic Source Parameter Imaging Constraints on The Structural Framework and its Implications for Geo-Hazard Occurrence in The Upper Benue Trough, NE Nigeria

Sebastian Abraham Sunu [1, 2] *, Adetola Sunday Oniku [2], Bello Yusuf Idi [2], Osita Chukwudi Meludu [2], Abbey Chukwuemeka Patrick [1], Lucky Peter Kenda [2, 3], Humphrey Beatrice Bomki [4]

[1] Department of Petroleum Chemistry & Physics American University of Nigeria (AUN) Yola
[2] Department of Physics, Modibbo Adama University, Yola, Adamawa State, Nigeria
[3] Department of Physics, Taraba State University, Jalingo
[4] Department of Physics, Federal University of Agriculture Mubi
**Corresponding author E-mail: abraham.sebastian@aun.edu.ng*

Received: April 9, 2026, Accepted: May 13, 2026, Published: May 27, 2026

Abstract

This study investigates the basement depth and structural framework of the Upper Benue Trough, northeastern Nigeria, using high-resolution aeromagnetic data integrated with Source Parameter Imaging (SPI) techniques to assess their implications for geo-hazard occurrence. The aeromagnetic data were processed using Oasis Montaj software 8.9 through standard procedures, including reduction to the equator and regional-residual separation, to enhance subsurface structural features. The SPI method, based on the analytic signal of magnetic sources, was employed to estimate depths to magnetic sources, revealing significant spatial variability ranging from approximately 98 m shallow depths to over 2200 m deeper depths. The results indicate a structurally complex terrain characterized by NE-SW and NW-SE trending fault systems, with deeper sedimentary depocenters concentrated in the central and southern parts of the study area and shallower basement highs along the margins. Integration of SPI-derived depths with lineament density analysis highlights zones of intense fracturing, deformation and structural weakness, which correspond to areas prone to geo-hazards such as flooding, subsidence, landslides, and erosion. The findings reveal that basement configuration and fault-controlled structures play a critical role in controlling geo-hazard susceptibility, providing a critical geophysical framework for improved risk assessment, land-use planning, and sustainable infrastructure development in the Upper Benue Trough.

Keywords: *SPI; Geo-Hazards; Basement Depth; Upper Benue Trough; Lineaments.*

1. Introduction

Determining basement depth is crucial in geophysical prospecting, especially in sedimentary basins, where it provides critical information on tectonic evolution, sediment thickness, geo-hazard occurrence, and mineral potential (Blakely, 1995; Kearey et al., 2002). In rift-related basins characterized by complex geological structures such as the Benue Trough of Nigeria, basement configuration plays an important role in controlling structural deformation, magmatic intrusions, and geo-hazard occurrence (Benkhelil, 1989; Guiraud & Bosworth, 1997). The Upper Benue Trough, particularly the Gongola and Yola arms, demonstrates a structurally complex framework of faults dominated by NE-SW, NW-SE, and ENE-WSW orientations. These structural trends are associated with extensional tectonics, basin subsidence, and subsequent tectonic reactivation (Guiraud & Bosworth, 1997). Aeromagnetic studies across the region have exposed that the basement is highly complex and undulating, with variations in depth reflecting heterogeneous crustal responses to rifting, magmatism, and tectonic processes. Such structural complexity has direct implications for geo-hazard occurrence, including ground instability, seismic activity, soil erosion, flooding, and fluid migration pathways.

Aeromagnetic techniques have proven to be cost-effective and reliable tools for investigating subsurface geological structures due to their sensitivity and accessibility to variations in magnetic properties (susceptibility) of rocks (Blakely, 1996; Telford et al., 1998; Salem et al., 2014). High-resolution aeromagnetic data are used to delineate faults, fractures, and lithological boundaries even in areas with limited surface vegetation exposure. Several studies in the Upper Benue Trough have successfully applied aeromagnetic techniques to estimate basement depth and sediment thickness, revealing depths ranging from less than 1 km to over 4.9 km in different parts of the basin. Simi-

larly, broader studies across the Benue Trough have reported basement depths varying from 1 km to 9 km, indicating significant spatial variability in basin architecture (Ofoegbu, 1985). Different quantitative techniques have been developed to estimate the depth to the top of magnetic sources in geophysical investigations (Blakely, 1995; Nabighian et al., 2005). These techniques may be applied in either the spatial domain or the frequency (wavenumber) domain. However, depth estimation in the frequency domain is generally considered more advanced and computationally efficient, as the convolution operations inherent in spatial analysis are transformed into simple multiplicative relationships through the application of the Fourier Transform (Bhattacharyya, 1966; Spector & Grant, 1970; Garcia-Abdeslem & Ness, 1994; Salem et al., 2014). Among these approaches, the spectral method proposed by Spector & Grant (1970) has become one of the most widely applied techniques for estimating the depth to magnetic sources in the frequency domain. This method has been extensively validated and applied in numerous studies, demonstrating its effectiveness in delineating subsurface structures and basement configurations (Shuey et al., 1977; Connard et al., 1983; Okubo et al., 1985; Blakely, 1988; Pedersen, 1991; Garcia-Abdeslem & Ness, 1994; Okubo & Matsunaga, 1994; Tanaka et al., 1999).

Among the various quantitative interpretation techniques, Source Parameter Imaging (SPI) has gained popularity due to its efficiency and reliability in estimating depth to magnetic (anomaly) sources. The SPI method is based on the analytic signal of magnetic anomalies and provides rapid depth estimation independent of magnetization direction, magnetic data without detailed inversion (Thurston & Smith, 1997; Silva et al., 2006). Accurate interpretation of these anomalies requires estimating the source parameters, particularly the depth and geometry of the causative bodies (Reid et al., 1990; Li & Oldenburg, 1998). Previous applications of SPI in the Benue Trough have demonstrated its effectiveness in mapping basement topography and identifying structural elements like faults, fractures, lithological boundaries, and intrusions. Ugwu, G. Z. & Alasi, T. K. (2016) investigated depth to magnetic sources and lineaments in the lower Benue trough using SPI techniques. Basement depths ranged from 2.5 km to 4.2 km, while shallow magnetic sources varied from 0.6 km to 0.9 km. Further regional studies by Odidi, I. G. et al. (2020) applied the SPI method to determine basement depths across parts of northeastern and central Nigeria, including portions of the Upper Benue Trough, Gongola Basin, and Yola arm. Their results revealed basement depths ranging from 0.12 km to 12.26 km, with shallower basement occurring in the northeastern region and deeper structures concentrated toward the southwest. These features are often associated with zones of structural weakness that may influence geo-hazard occurrence, including landslides, subsidence, and geothermal activity.

In the upper Benue trough, numerous studies have examined basin geometry and configurations using aeromagnetic data. However, integrated investigations of basement depth, especially those addressing geo-hazard implications, remain limited. This study aims to determine basement depth using aeromagnetic Source Parameter Imaging (SPI) and assess its relationship with structural features that may influence geo-hazard occurrence in the region, focusing directly on the link between basement depth and geo-hazard risk.

2. Location, Geology, and Tectonic Setting of The Study Area

The study area (Figure 1) encompasses Adamawa State and Taraba State in northeastern Nigeria, forming part of the Upper segment of the Benue Trough. It lies between latitudes 7°-11°N and longitudes 9°-14°E, bounded by the Nigerian Basement Complex and extending towards the Cameroon border. This region represents a transitional zone between sedimentary basins and crystalline basement terrains and includes notable physiographic features such as the Mambilla Plateau (Benkhelil, 1989).

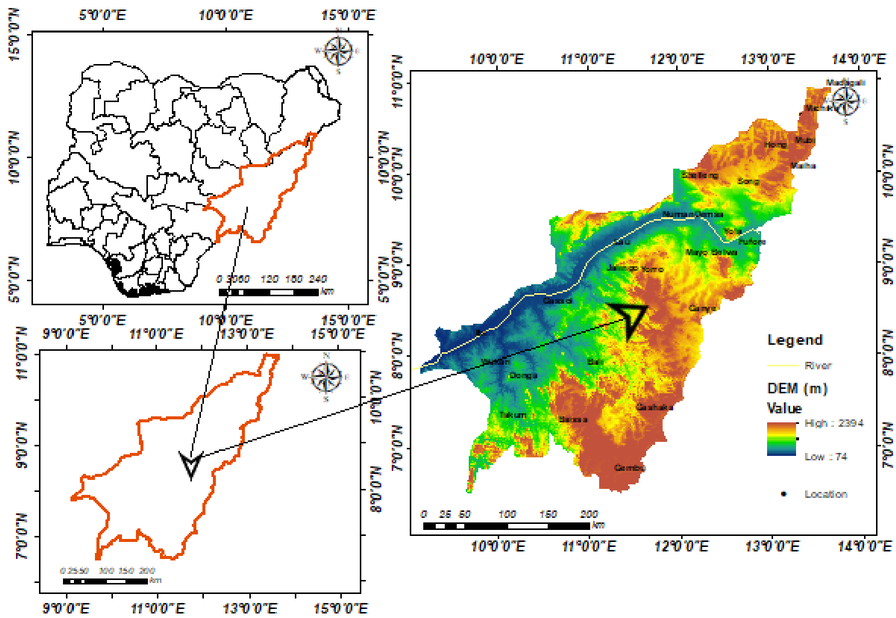

Fig. 1: Study Area Map Prepared Using Arcgis 10.6 (sunu et al., 2026).

Geologically, the study area (Figure 2) is characterized by Cretaceous sedimentary rocks such as sandstones, shales, and limestones, overlying Precambrian basement composed of granites, gneisses, and migmatites, with exposures in uplifted zones. Volcanic and intrusive rocks linked to the Cameroon Volcanic Line indicate Cenozoic magmatic activity. Tectonically, the Upper Benue Trough developed as a rift basin during the Early Cretaceous in response to the opening of the South Atlantic and the breakup of Gondwana, with NE-SW trending fault systems controlling subsidence, sedimentation, and structural architecture. Subsequent tectonic reactivation and volcanism further modified the basin, resulting in a complex interplay of rifting, faulting, and magmatic processes (Yenne et al. 2025; Benkhelil, 1989; Fairhead & Binks, 1991).

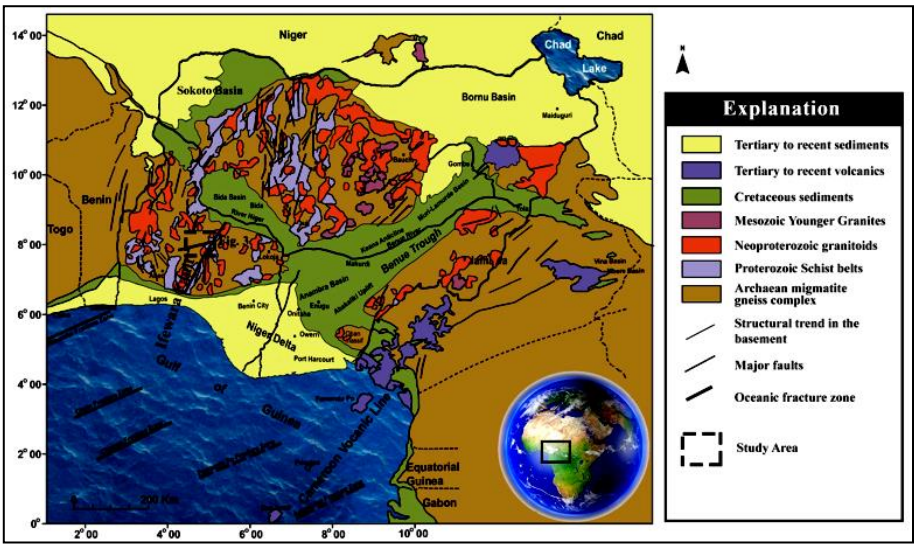

Fig. 2: Generalized Geology of Nigeria Showing the Geology of the Study Area (Modified After Benkhelil et al. 1998; Arthaud et al. 2008)

3. Methodology

3.1. Data acquisition

High-resolution aeromagnetic total magnetic intensity (TMI) data made up of forty-six (46) sheets covering Adamawa/Taraba of the Upper Benue Trough were obtained from the Nigerian Geological Survey Agency (NGSA). The dataset typically consists of Total Magnetic Intensity (TMI) measurements acquired along flight lines of 500 m with consistent tie spacing of 5000 m and altitude of 80 m, in the NW-SE orientations, providing detailed coverage of subsurface magnetic variations. Magnetic data corrections were carried out by Fugro Airborne Surveys. The geomagnetic gradient was removed using the January 2005 International Geomagnetic Reference Field (IGRF) model referenced to the World Geodetic System 1984 ellipsoid. The aeromagnetic data were geo-referenced to the Universal Transverse Mercator (UTM) coordinate system WGS 1984 32N for comparative study with the geological map of the area. To interpret more flexibly, the total magnetic intensity value T was stripped of 33000 nT. The value of 33000 nT was re-added to each value of T to obtain the actual values of total magnetic intensity (T) of the study area. Aeromagnetic data are particularly useful for mapping basement structures due to their sensitivity to contrasts in magnetic susceptibility between basement rocks and overlying sediments.

3.2. Data processing

The aeromagnetic data were processed using standard geophysical procedures to enhance structural features and prepare the data for quantitative interpretation. The data were enhanced and prepared using various filtering techniques such as Reduction to equator (RTE) to reduce the effect the effects of inclination and declination, ensuring anomaly symmetry appropriate for spectral interpretation and Regional and Residual separation was applied on the TMI data (Figure 3) to isolate the short-wavelength magnetic sources of interest associated with near-surface and intermediate magnetic sources from long-wavelength regional trends caused by deeper crustal bodies. The Total Magnetic Intensity (TMI) map of the study area (Figure 3) indicates spatial variation in the Earth's magnetic field as a result of differences in magnetic susceptibility (χ) between subsurface geological formations. The interaction between Earth's magnetic field (H_0) and subsurface rock materials leads to the acquisition of induced magnetization by different rock units, given in equation 1:

$$M = \chi H_o \tag{1}$$

M = magnetization (A/m)
χ = magnetic susceptibility
H_0 = Earth's magnetic field
Rocks with higher magnetic susceptibility, such as igneous extrusions and intrusions, basement rocks rich in magnetite, become more strongly magnetized and produce high-amplitude magnetic (sources) anomalies; typically represented in reds/pinks on the TMI map (Figure 3). While rocks with low-susceptibility materials, such as sedimentary rocks, sandstone, or shale, produce weaker anomalies, indicated by blues/greens (Figure 3) (Blakely, 1995; Kearey et al., 2002). The observed magnetic field is therefore the sum of the regional geomagnetic field and the induced field from subsurface sources, expressed in equation 1:

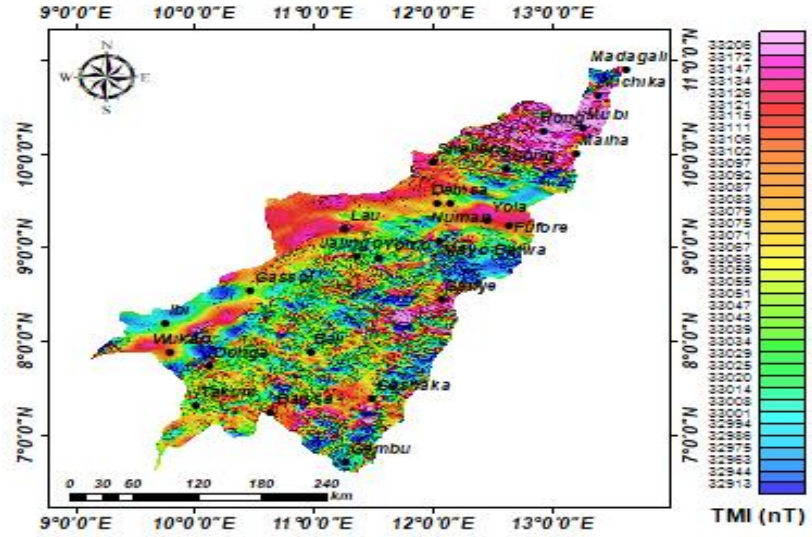

Fig. 3: Total Magnetic Intensity (TMI) of the Study Area.

$$B = \mu_o(H_o + M) \tag{2}$$

B =Magnetic Flux Density (Total Magnetic Field) Unit: Tesla (T).
μ_o = Magnetic Permeability of Free Space.
$\mu_o = 4\pi \times 10^{-7} H/m$

Where μ_o acts as a scaling factor converting magnetic field strength into flux density.
According to Hinze et al. (2013), magnetic susceptibility contrasts are therefore crucial in interpreting basement topography, structural orientations, and geo-hazard-prone zones within the study area.

3.3. Regional and residual separation

Regional and residual separation of magnetic data is a fundamental processing step in aeromagnetic interpretation used to distinguish deep-seated geological features from shallow subsurface anomalies (Blakely, 1995; Telford et al., 1998; Kearey et al., 2002). The regional magnetic field (figure 4) represents broad, smooth anomalies produced by large-scale and deep crustal structures, long-wavelength basement variations, and the Earth's main magnetic field trend, whereas the residual magnetic field contains short-wavelength anomalies associated with localized and shallower sources such as faults, fractures, lithologic contacts, intrusions, and near-surface basement irregularities (Blakely, 1995; Hinze et al., 2013; Telford et al., 1998). Separation is commonly achieved through filtering techniques such as polynomial fitting, upward continuation, wavelength filtering, Fourier domain analysis, or trend surface analysis, where the regional component is estimated and removed from the total magnetic intensity data to isolate the residual anomalies (Spector & Grant, 1970; Salem et al., 2014). This enhances the resolution of local structural features and improves geological interpretation, especially in sedimentary basins where shallow structures control mineralization, groundwater occurrence, hydrocarbon trapping, and tectonic deformation (Ofoegbu, 1985; Benkhelil, 1989).

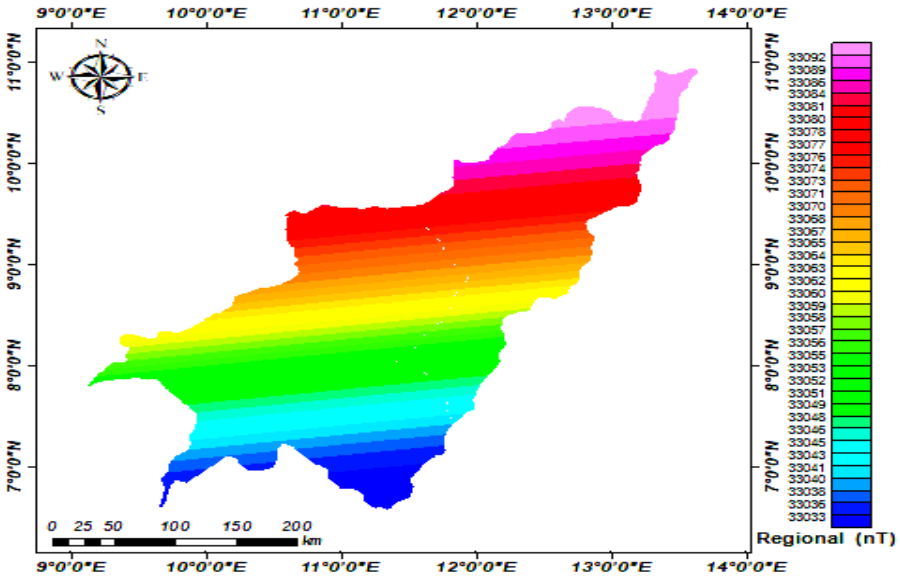

Fig. 4: Regional Magnetic Map of the Study Area.

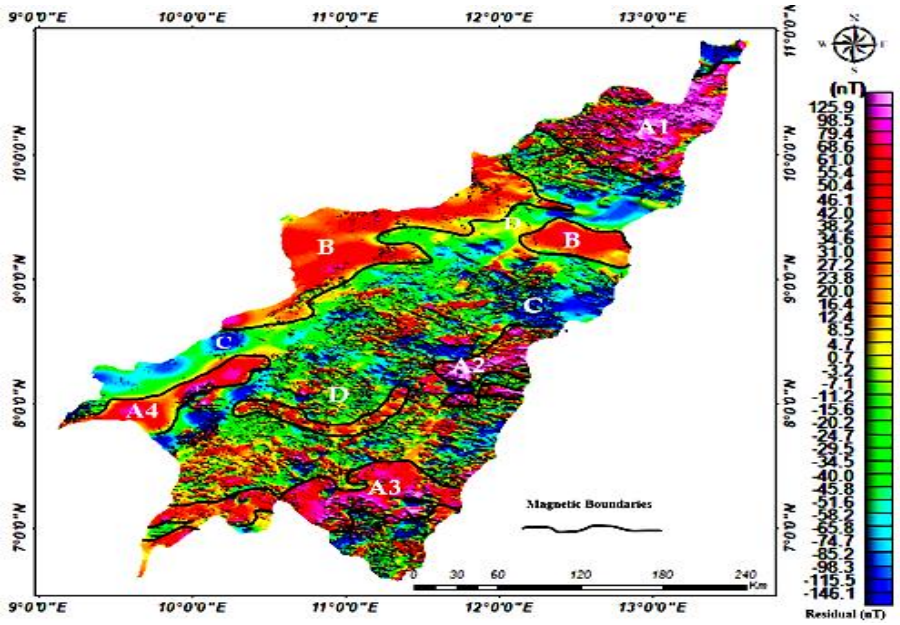

Fig. 5: Residual Magnetic Map of the Study Area.

3.4. Reduction to the equator

Reduction to the Equator (RTE) (Figure 6) is a magnetic data transformation technique applied to aeromagnetic anomalies acquired in low magnetic latitude regions, where the Earth's magnetic field is nearly horizontal. In such areas, magnetic anomalies produced by subsurface bodies are often asymmetrical and spatially displaced from their causative sources due to the combined effects of low geomagnetic inclination and declination.

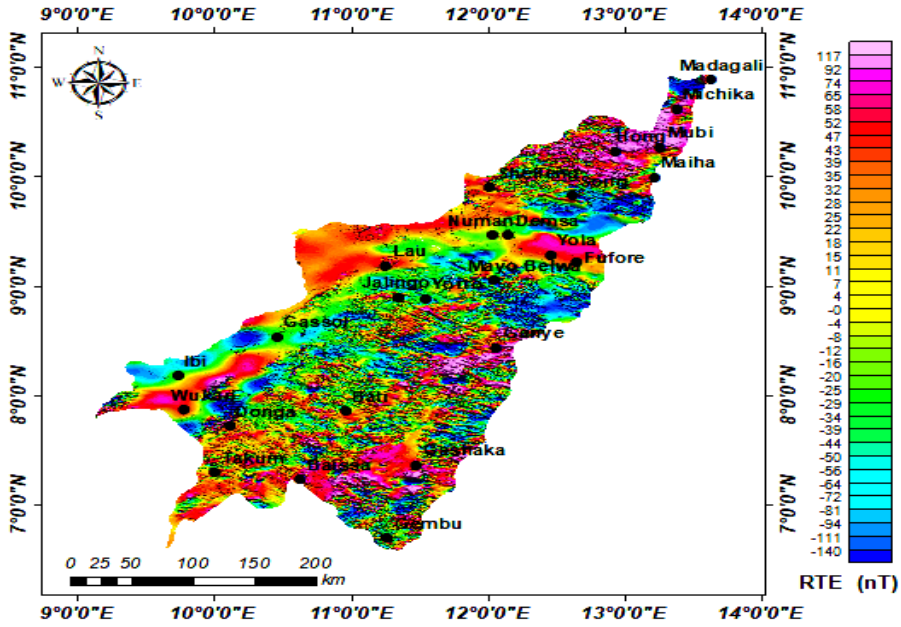

Fig. 6: Reduction to Equator Map of the Study Area.

RTE corrects this distortion by mathematically transforming the magnetic field as if both the inducing geomagnetic field and the magnetization vector were horizontal and aligned with the equator, thereby repositioning anomalies closer to their actual geological sources (Blakely, 1995; Nabighian et al., 2005). This process improves anomaly symmetry and enhances the interpretation of structural features such as faults, contacts, intrusions, and basement boundaries. RTE is especially important in tropical regions like Nigeria, where low magnetic inclinations make conventional magnetic interpretation difficult, and it serves as an alternative to Reduction to Pole (RTP), which becomes unstable near the magnetic equator (Salem et al., 2014; MacLeod et al., 1993).

3.5. Source parameter imaging (SPI)

The Source parameter imaging (SPI) technique (Thurston and Smith, 1997) was applied in this study to calculate depth to magnetic sources in the study area. This method offers rapid and automatic depth estimation over the study area characterized by complex geologic features. The local wave number of the gradients of the magnetic field from the analytic signal computes the SPI. The method is rooted in potential field theory and assumes simple source geometries (such as contacts, dykes, cylinders). Let the observed magnetic sources (anomaly) be given as:

$$F(x, y, z) \quad (3)$$

For a given 2D source (dykes or contacts), the magnetic field may be expressed as a function of horizontal position and depth, given as:

$$F(x, z)\alpha\, ln((x - x_o)^2 + z^2) \quad (4)$$

Where,
xo = anomaly or source location
z = depth to anomaly or source
Source parameter imaging explores spatial derivatives of the total magnetic field. The first-order spatial derivative is given in equation 5

$$\frac{\partial F}{\partial x}, \frac{\partial F}{\partial y}, \frac{\partial F}{\partial z} \quad (5)$$

Where the horizontal gradient magnitude (HGM) and Analytic signal (AS) are expressed in equations 6 and 7:

$$HGM = \sqrt{\left(\frac{\partial F}{\partial x}\right)^2 + \left(\frac{\partial F}{\partial y}\right)^2} \quad (6)$$

$$AS_1(x, z) = \frac{\partial F(x,z)}{\partial x} - j\frac{\partial F(x,z)}{\partial z} \quad (7)$$

Where,

AS_1 = magnitude of analytic signal

HGM = Horizontal gradient magnitude

∂F = partial derivative of the total magnetic field

$\frac{\partial F}{\partial x}$ = Magnetic field gradient in the x-direction (east–west direction)

$\frac{\partial F}{\partial y}$ = Magnetic field gradient in the y-direction (north–south direction)

$\frac{\partial F}{\partial z}$ = Vertical magnetic gradient (change with depth/elevation)

x, y, z = Cartesian coordinates representing horizontal and vertical spatial directions

AS_1(x, z) = magnitude of the anomalous total magnetic field,

j = imaginary number,

z and x are Cartesian coordinates for the vertical direction and horizontal direction perpendicular to strike, respectively. Hibert transform pair may be expressed in equation 8 as:

$$\frac{\partial F(x,z)}{\partial x} \Leftrightarrow -j\frac{\partial F(x,z)}{\partial z} \quad (8)$$

$$AS = \sqrt{\left(\frac{\partial F}{\partial x}\right)^2 + \left(\frac{\partial F}{\partial y}\right)^2 + \left(\frac{\partial F}{\partial z}\right)^2} \quad (9)$$

AS = analytic signal amplitude

$\frac{\partial F}{\partial x}$ = Magnetic field gradient in the x-direction (east-west direction)

$\frac{\partial F}{\partial y}$ = Magnetic field gradient in the y-direction (north-south direction)

$\frac{\partial F}{\partial z}$ = Vertical magnetic gradient (change with depth/elevation)

x, y, z = Cartesian coordinates representing horizontal and vertical spatial directions

Equation 9 is independent of magnetization direction and peaks over source edges.

Where ⇔ = Hilbert transformation pair, Thurston and Smith (1997) defined local wave number expressed in equation 10 as k_1

$$k_1 = \frac{\partial}{\partial x}\left(tan^{-1}\left(\frac{\frac{\partial F}{\partial z}}{\frac{\partial F}{\partial x}}\right)\right) \quad (10)$$

k_1 = First-order local wave number

$\frac{\partial}{\partial x}$= Partial derivative with respect to the x-direction

tan^{-1} = Inverse tangent (arctangent) function

$\frac{\partial F}{\partial x}$ =Vertical derivative of magnetic field

$\frac{\partial F}{\partial x}$ =Horizontal derivative of magnetic field

The Hilbert transform pair in equation (8) is applied to the analytic signal in equation (7); the vertical-derivative operators are linear, and so the vertical derivative of equation (7) will give the Hilbert transform pair in equation 11:

$$\frac{\partial^2 F(x,z)}{\partial z \partial x} \Leftrightarrow -\frac{\partial^2 F(x,z)}{\partial^2 z} \tag{11}$$

F(x, z) = Magnetic field as a function of horizontal position and depth

$\frac{\partial^2 F(x,z)}{\partial z \partial x}$ = Mixed second-order derivative with respect to x and z

$\frac{\partial^2 F(x,z)}{\partial^2 z}$ = Second vertical derivative of the magnetic field

$\Leftrightarrow$ = Represents Hilbert transform pair relationship

Thus, the analytic signal is defined based on second-order derivatives $\mathrm{AS}_2(\mathrm{x}, \mathrm{z})$

$$AS_2(x,z) = \frac{\partial^2 F(x,z)}{\partial z \partial x} - j\frac{\partial^2 F(x,z)}{\partial^2 z} \tag{12}$$

This yields the second-order local wave number k2:

$$k^2 = \frac{\partial}{\partial x}\left(tan^{-1}\left(\frac{\frac{\partial^2 F}{\partial^2 z}}{\frac{\partial^2 F}{\partial z \partial x}}\right)\right) \tag{13}$$

The vertical and horizontal gradient of a sloping contact model (Nabighian 1972) is expressed in equations 14 and 15:

$$\frac{\partial F}{\partial x} = 2Kf_c \sin d \frac{h_c cos(2I-d-90)+x\, sin(2I-d-90)}{h_c^2+x^2} \tag{14}$$

$$\frac{\partial F}{\partial x} = 2Kf_c \sin d \frac{x\, cos(2I-d-90)+h_c sin(2I-d-90)}{h_c^2+x^2} \tag{15}$$

Where,
K = susceptibility contrast at the contact,
F = magnitude of the Earth`s magnetic field (the inducing field),
d = dip (measured from the positive x-axis),
α = angle between the positive x-axis and magnetic north,
I = ambient-field inclination of the contact, and all trigonometric arguments are in degrees $\mathrm{c} = 1 - \cos^2\alpha \mathrm{i} \sin^2$ and $\tan\mathrm{I} = \frac{\sin\mathrm{i}}{\cos\alpha}$

The origin of the profile line (x = 0) is directly over the edge defined by the coordinate system. The expression for the magnetic-field anomaly due to a dipping thin sheet is given by equation 16:

$$F(x,z) = 2Kf_{cw} \sin d \frac{h_1 sin(2I-d-90)+x\, cos(2I-d-90)}{h_c^2+x^2} \tag{16}$$

$$k_1 = \frac{(n_k+1)h_k}{h_k^2+x^2} \tag{17}$$

$$k_2 = \frac{(n_k+2)h_k}{h_k^2+x^2} \tag{18}$$

Where
n_k is the SPI structural index (subscript k = c, t or h),
$n_c = 0$, $n_t = 1$ and $n_h = 2$
for the contact, thin sheet, and horizontal cylinder models, respectively. From equations 5 and 10 above, it is evident that the first- and second-order local wave numbers are independent of the susceptibility contrast, the dip of the source, the inclination, declination, and the strength of the Earth's magnetic field.
For 2D structures, equations 17 and 18 may be simplified and written as follows:

$$k(x) = \frac{\left(\frac{\partial^2 F}{\partial x \partial z}\frac{\partial F}{\partial x} - \frac{\partial^2 F}{\partial x^2}\frac{\partial F}{\partial z}\right)}{\left(\frac{\partial F}{\partial x}\right)^2 + \left(\frac{\partial F}{\partial z}\right)^2} \tag{19}$$

F=Magnetic field intensity or magnetic anomaly field

$\frac{\partial F}{\partial x}$ =Partial Derivative Magnetic field in the x-direction (east–west direction)

$\frac{\partial^2 F}{\partial x^2}$ = Second vertical derivative of the magnetic field

$\frac{\partial F}{\partial z}$= Partial Derivative Magnetic field in the x-direction (north–south direction)

Where the inverse of the local wave number k is the depth to the source, expressed as in equations 20 and 21:

$$z = \frac{1}{k(x,y)} \tag{20}$$

$$Depth = \frac{1}{local.wavenumber} \tag{21}$$

z = depth, k(x,y) = local wave number
The application of SPI assumes that: Geometry of the source bodies must be uncomplicated, higher order derivatives are affected by noise, require filtering, and quality data.

4. Results and Discussion

4.1. Analytic signal (AS)

Analytic signal map (Figure 7) revealed strong magnetic anomalies across the Upper Benue Trough, clearly differentiating the thick sediment-filled Benue Trough from the surrounding crystalline basement complexes (Nabighian, 1972; Blakely, 1995). High analytic signal amplitudes observed within the Northern Basement Complex and Northeastern Basement Complex (Figure 5) indicate shallow magnetic anomalies associated with highly magnetized crystalline rocks, basement uplifts, igneous intrusions, and structurally deformed zones (Salem et al., 2014). In contrast, the relatively low amplitudes across the central Benue Trough correspond to deeper magnetic anomalies, reflecting thicker sedimentary cover and greater basement depths. This observation is consistent with SPI results, which suggest deeper basement configurations beneath the trough and shallower basement conditions toward the adjoining basement terrains (Thurston & Smith, 1997). Tectonically, the spatial distribution of analytic signal amplitudes reflects the rift-related evolution of the Upper Benue Trough. The elongated low-amplitude zone trending NE-SW corresponds to the main sedimentary depocenter formed during Cretaceous crustal extension associated with the opening of the South Atlantic (Wright, 1968; Benkhelil, 1989). Meanwhile, sharp amplitude gradients along the basin margins mark major basement faults and structural contacts that controlled subsidence, magmatic emplacement, and sediment accumulation (Guiraud & Bosworth, 1997). These structural discontinuities confirm that the tectonic architecture of the Upper Benue Trough is strongly influenced by basement-involved faulting and differential crustal deformation (Benkhelil, 1989; Guiraud & Bosworth, 1997).

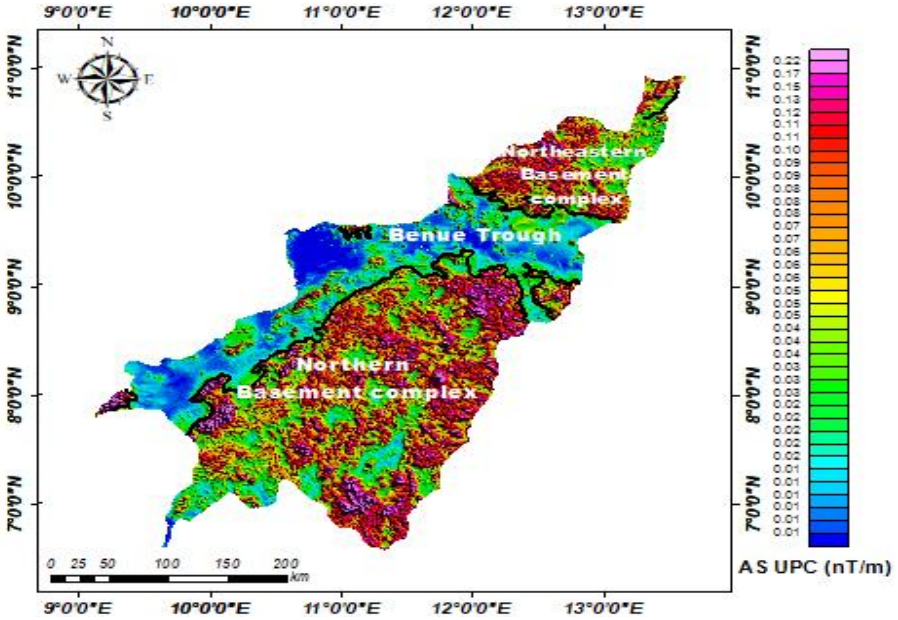

Fig. 7: Analytic Signal (AS) Map of the Study Area.

4.2. Source parameter imaging (SPI)

Source Parameter Imaging (SPI) map of the study region (Figure 8) shows spatial variation in estimated depths to magnetic sources, ranging from shallow (blue-green colors, 98.38 m) to very deep (red-pink colors, 2282.87 m). A prominent NE-SW trending deep zone in the central part of the study area around Numan, Demsa, Yola, and Fufore, and in the southern part around Wukari, Ibbi, and Gossol, suggests a structurally controlled trough or sedimentary depocenter, possibly related to regional faulting and basement subsidence that hosted thick sediment relative to the surrounding basement (Sunu et al., 2026). An intermediate depth exists between 300 -700 m, which is yellow-orange-green colors. This marks the transition from basement highs to depressions, and is commonly associated with steep basement slopes, Fracture concentration zones, and lithological boundaries. In contrast, the surrounding shallow zones (98.98 m blue to cyan to green) likely represent basement uplifts, structural highs, or near-surface igneous intrusions or volcanic rocks known as the basement complex associated with magnetically susceptible rocks with reduced sediment cover, possible tectonic uplift relative to adjacent deeper zones (Sunu et al., 2026). The pattern indicates a tectonically complex terrain with significant basement relief, with deeper sections potentially favorable for sediment accumulation and shallower anomalies associated with structural or lithologic contrasts and tectonically weakened zones-factors that collectively influence the spatial distribution of geo-hazards such as flooding, landslides, river incision, erosion, and structural instabilities. The central and northeastern segments of the study area (highlighted in purple, pink, and red) represent deep magnetic sources, reflecting: Fault-bounded basement depressions, Rift-related subsidence zones associated with the

Benue Trough system with thick sedimentary cover, deep fracturing and concealed tectonic lineaments, deep basinal structures often coincide with Low-lying plains and thick weathered/sedimentary layers with high porosity, and high groundwater accumulation.

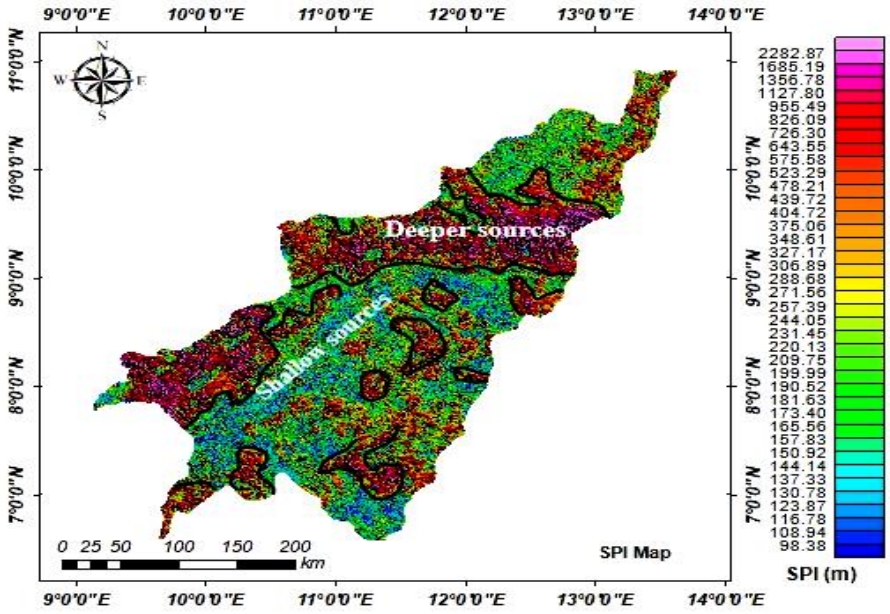

Fig. 8: Source Parameter Imaging (SPI) Map of the Study Area.

4.3. Structural interpretation

The SPI-derived depth map (Figure 8) was integrated with the residual magnetic anomaly map to delineate structural features such as Faults, Basement highs and depressions, and lineament trends. These features were interpreted based on anomaly patterns, gradients, and depth variations. Structural trends were analyzed using a directional rose to identify dominant orientations consistent with regional tectonics. Lineaments and the Faults of the study area (Figure 9a) delineate a network of structurally controlled discontinuities (Thurston & Smith, 1997; Blakely, 1995) distributed across the study area, with significant concentrations in the central and southern parts, indicating zones of tectonic deformation and crustal weakness. The faults are generally aligned along the inferred basement-sedimentary boundary, highlighting the structural transition between the crystalline basement and the sedimentary sequences of the Benue Trough (Figure 9a). The corresponding rose diagram indicates a dominant NW-SE orientation, with minor NE-SW and N-S trends (Figure 9b), suggesting that fault development was controlled by multiple tectonic stress regimes associated with rifting and subsequent reactivation events.

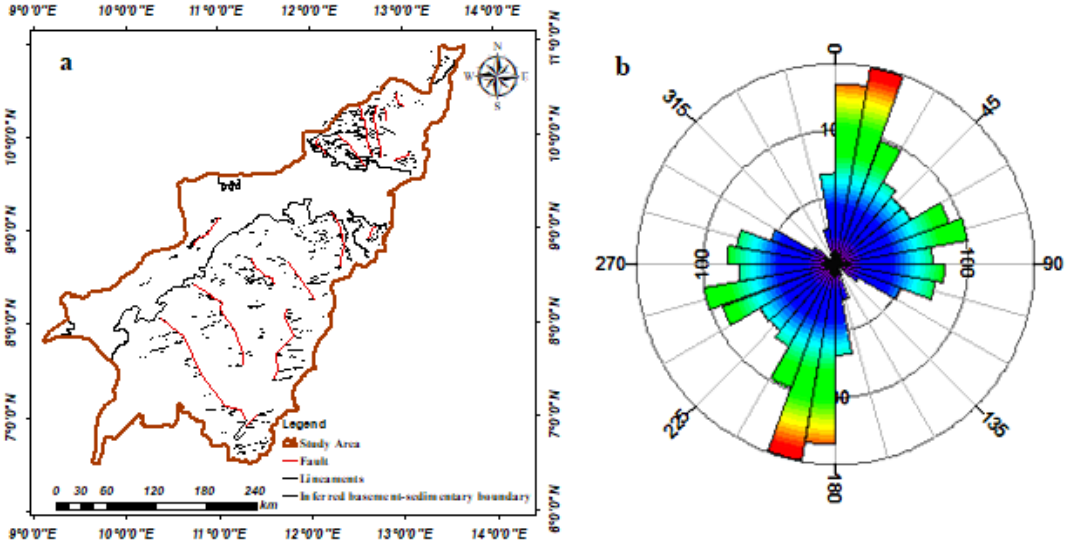

Fig. 9: (a) Lineament Density Map and Corresponding of the Adamawa-Taraba Region Within the Benue Trough (b) Rose Diagram Showing Dominant NE-SW to ENE-WSW Structural Trends with Subordinate NW-SE Orientations, Indicative of Regional Tectonic Controls and Fracture Patterns.

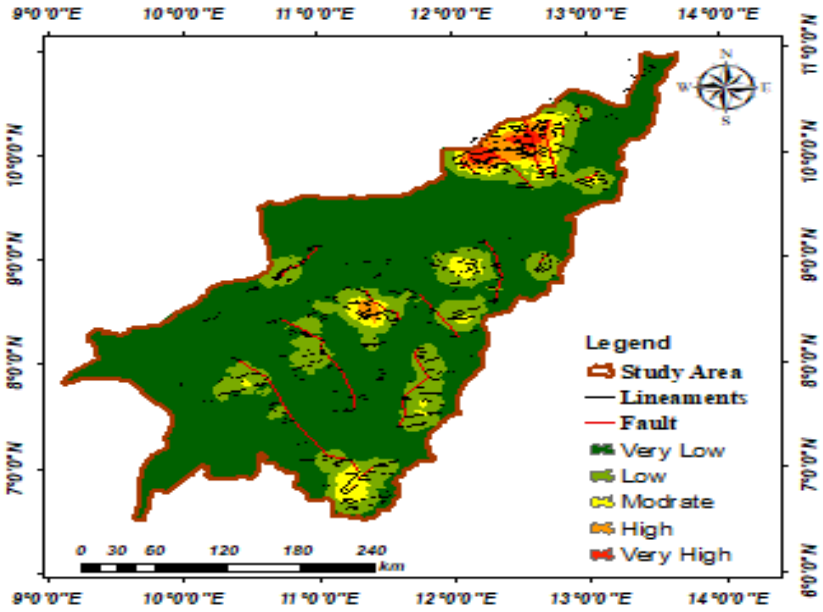

Fig. 10: Lineament Density Map of the Study Area.

4.4. Geo-hazard implications of SPI constraints with structural elements analysis

Source Parameter Imaging (SPI) map integrated with lineament density (Figure 11) demonstrated significant spatial variations, complex structural configurations, and basement depth across the study area. High lineament density zones, particularly around Michika, Madagali, Sheleng Gashaka, Gembu, and Donga, indicate severely fractured and faulted terrains that serve as zones of structural weakness. These areas are highly susceptible to geo-hazards such as ground instability, fault reactivation, and landslides, especially where topographic elevation is significant. Moderate density zones, observed around Jalingo, Lau, Ganye, and Mayo-Belwa, exhibit intermediate structural deformation and are associated with localized hazards such as erosion and minor subsidence. In contrast, low to very low lineament density regions, including Demsa, Yola, Fufore, Wukari, Lau, Ibbi, and Gossol, are relatively stable and less prone to structurally induced hazards, although surface processes like flooding and erosion may still occur. The SPI-derived depth estimates further identified the geo-hazard assessment by indicating variations in sediment thickness and basement configuration. Shallow basement areas are more prone to surface deformation and potential seismic sensitivity, while deeper basement zones with thick sedimentary cover are associated with increased risks of subsidence, compaction, and flooding. Regions where high lineament density coincides with greater basement depths represent the most vulnerable zones due to the combined effects of structural weakness and sedimentary loading.

4.5. SPI sensitivity analysis

The Source Parameter Imaging (SPI) map enables an estimate of the depth to magnetic anomalies based on the local gradients of aeromagnetic sources. Sensitivity analysis of the SPI map involves evaluating how variations in magnetic response reflect variations in lithology, basement architecture, structural deformation, sediment thickness, and rifting intensity across the study area. The analysis also assesses the reliability and geological implications of shallow and deep magnetic responses (Thurston & Smith, 1997; Salem et al., 2008). The SPI depth solutions in the map range from approximately 98 m to 2283 m, suggesting powerful spatial variability in magnetic anomaly distribution and complex subsurface structure.

4.5.1. Observed SPI attributes from basement depth variations

The SPI map shows the following attributes:
1) Shallow magnetic sources (blue-green colors; ~ 98 - 400 m).
2) Moderate depths (~ 400 - 900 m).
3) Deep magnetic sources (pink-purple colors; > 1000 - 2200 m).

And this resulted in the following observations from the SPI map:
Strong lateral depth variations, extended depth trends, structurally oriented anomalies, and sharp SPI gradients.

4.5.2. Sensitivity to structural discontinuities

The SPI map clearly deciphers sharp lateral changes between shallow and deep magnetic zones. These transitions are interpreted as: faults, fractures, shear zones, lithologic contacts, and tectonic boundaries (Nabighian et al., 2005). The elongated magnetic orientation trending majorly NE-SW and primarily E-W indicates a structurally controlled magnetic indicator. Such trends are consistent with regional tectonic features associated with the structural evolution of the Benue Trough (Benkhelil, 1989).
The sensitivity of SPI to structural discontinuities is evident because:

- Depth values change abruptly across lineaments.
- Magnetic gradients are stronger near fault contacts.
- Structural boundaries produce magnetic susceptibility contrasts across edges (Kearey et al., 2002).

Therefore, the SPI method effectively enhances tectonic lineaments and basement offsets that may not be visible in raw magnetic intensity data.

4.5.3. Sensitivity to magnetic susceptibility contrast

SPI depth estimation depends strongly on the magnetic susceptibility contrast between adjacent rock units. Areas with strong magnetic contrasts generate sharper gradients and more reliable depth solutions (Salem et al., 2008). In the SPI map (Figure 8), isolated circular and elongated shallow sources likely correspond to highly magnetic intrusive bodies (Igneous), while smoother deep zones represent weakly magnetic sedimentary formations. High-susceptibility rocks such as granites, dolerites, basalts, and ferruginous intrusions produce stronger magnetic responses and shallower SPI solutions (Telford et al., 1990). Low magnetic susceptibility sediments produce weaker sources and deeper SPI estimates. This suggests that the SPI algorithm is highly responsive to lithologic variations and magnetic mineral concentration.

4.6. Analytical discussion of the SPI map superimposed on drainage density

The superimposed Source Parameter Imaging (SPI) map and drainage density map (Figure 11) suggest a powerful spatial relationship between subsurface structural orientation and surface hydrological attributes within the study area. The integration of SPI-derived magnetic basement depths with drainage density distribution provides important features into tectonic control, lithologic variations, structural deformation, groundwater occurrence, erosion processes, and landscape evolution. The observed relationship reveals that subsurface geologic features significantly influence surface drainage organization and geomorphological development (Ndikum & Tabod, 2024; Eze et al., 2024).

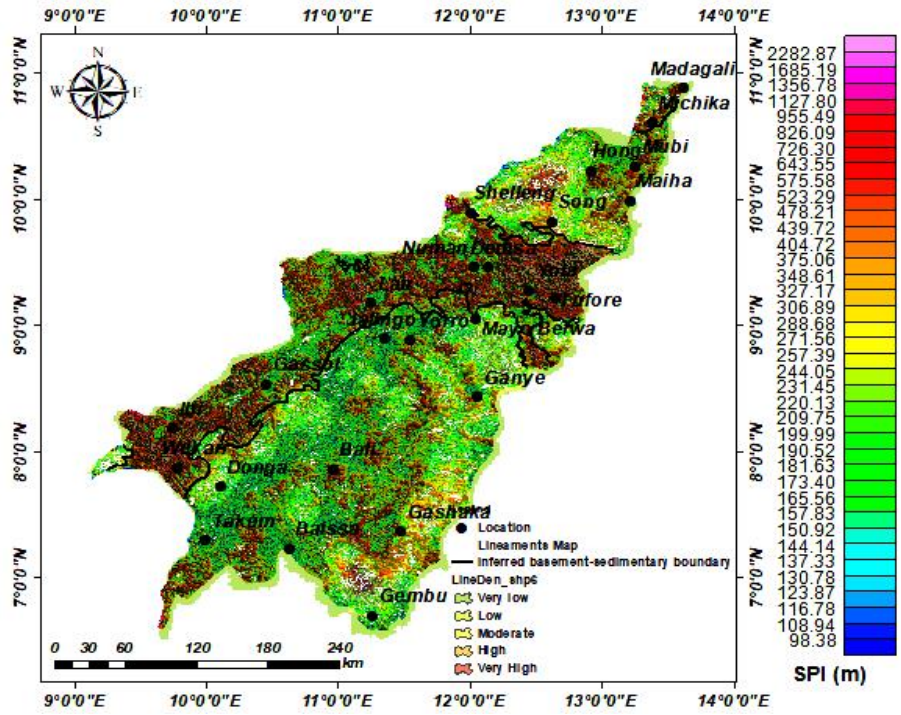

Fig. 11: Depth Estimation from Source Parameter Imaging (SPI), the Colour Bar Indicates the Depth Estimates in Meters (M).

5. Conclusions

The integration of Source Parameter Imaging (SPI) constrained with the structural map of the study area reveals complex structural distribution dominated by NE - SW and NW - SE trending basement-controlled faults, as indicated by lineament density, which is the primary control on geo-hazard occurrence, reflecting the regional rifting and evolution of the Benue trough, while basement depth influences the type and intensity of these hazards. Areas characterized by high fracture density combined with deep sedimentary cover are identified as the most vulnerable hazard zones due to the influence of structural weakness in subsurface conditions. Therefore, integrating basement depth with structural analysis provides a reliable framework for assessing geo-hazard susceptibility in the Upper Benue Trough and reveals essential insights for effective urban planning, infrastructure development, and disaster risk management.

Acknowledgement

The author would want to extend his profound gratitude to Prof. Adetola Sunday Oniku and Prof. Bello Yusuf Idi, my Ph.D. supervisors and other co-researchers, for providing expert academic guidance and moral support. The author also wishes to thank the Nigerian Geological Survey Agency (NGSA) and USGS for making total magnetic intensity aeromagnetic data and SRTM DEM data available for this study.

References

[1] Arthaud MH, Caby R, Fuck RA, Dantas EL, Parente CV (2008). Geology of the northern Borborema Province, NE Brazil, and its correlation with Nigeria, NW Africa. Geol Soc Lond Spec Publ 294(1):49–67. https://doi.org/10.1144/ sp294.4.

[2] Blakely, R. J. (1995). *Potential Theory in Gravity and Magnetic Applications*. Cambridge University Press. https://doi.org/10.1017/CBO9780511549816.

[3] Blakely, R. J. (1988). Curie temperature isotherm analysis and tectonic implications of aeromagnetic data from Nevada. *Journal of Geophysical Research, 93*(B10), 11817–11832. https://doi.org/10.1029/JB093iB10p11817.

[4] Benkhelil J, Mascle J, Guiraud M (1998). Sedimentary and structural characteristics of the Cretaceous along the Co ˆte D'Ivoire–Ghana transform margin and the Benue trough: A comparison. In: Mascle J, Lohmann GP, Moullade M et al (eds) Proceedings of the ocean drilling program, scientifi c results, vol 159. Ocean Drilling Program, College Station, pp 93–99. https://doi.org/10.2973/odp.proc.sr.159.007.1998.

[5] Benkhelil, J. (1989). The origin and evolution of the Cretaceous Benue Trough, Nigeria. *Journal of African Earth Sciences, 8*(2–4), 251–282. https://doi.org/10.1016/S0899-5362(89)80028-4.

[6] Connard, G., Couch, R., & Gemperle, M. (1983). Analysis of aeromagnetic measurements from the Cascade Range in central Oregon. *Geophysics, 48*(3), 376–390. https://doi.org/10.1190/1.1441476.

[7] Eze, O. E., Okiwelu, A. A., Ekwok, S. E., et al. (2024). Delineation of deep-seated crustal structures from magnetic data in the southeastern part of the Niger Delta basin, Nigeria. *Frontiers in Earth Science*, 12, 1439199. https://doi.org/10.3389/feart.2024.1439199.

[8] Fairhead, J. D., & Binks, R. M. (1991). Differential opening of the Central and South Atlantic Oceans and the opening of the West African rift system. *Tectonophysics, 187*(1–3), 191–203. https://doi.org/10.1016/0040-1951(91)90419-S.

[9] Guiraud, R., & Bosworth, W. (1997). Senonian basin inversion and rejuvenation of rifting in Africa and Arabia: Synthesis and implications to plate-scale tectonics. *Tectonophysics, 282*(1–4), 39–82. https://doi.org/10.1016/S0040-1951(97)00212-6

[10] García-Abdeslem, J., & Ness, G. E. (1994). Variations of Curie depth in southern Mexico using spectral analysis of aeromagnetic data. *Geophysics, 59*(3), 449–456.

[11] Hinze, W. J., Von Frese, R. R. B., & Saad, A. H. (2013). *Gravity and magnetic exploration: Principles, practices, and applications*. Cambridge University Press. https://doi.org/10.1017/CBO9780511843129.

[12] Li, Y., & Oldenburg, D. W. (1998). 3-D inversion of magnetic data. Geophysics, 63(1), 109–119. https://doi.org/10.1190/1.1444302.

[13] Kearey, P., Brooks, M., & Hill, I. (2002). *An introduction to geophysical exploration* (3rd ed.). Blackwell Science.

[14] MacLeod, I. N., Jones, K., & Dai, T. F. (1993). 3-D analytic signal in the interpretation of total magnetic field data at low magnetic latitudes. *Exploration Geophysics, 24*(4), 679–688. https://doi.org/10.1071/EG993679.

[15] Nabighian, M. N., Grauch, V. J. S., Hansen, R. O., LaFehr, T. R., Li, Y., Peirce, J. W., Phillips, J. D., & Ruder, M. E. (2005). The historical development of the magnetic method in exploration. *Geophysics*, 70(6), 33ND–61ND. https://doi.org/10.1190/1.2133784

[16] Ndikum, E. N., & Tabod, C. T. (2024). Applying Source Parameter Imaging (SPI) to aeromagnetic data to estimate depth to magnetic sources in the Mamfe Sedimentary Basin. International Journal of Geosciences, 15, 1–11. https://doi.org/10.4236/ijg.2024.151001

[17] Nabighian, M. N. (1972). The Analytic Signal of Two-Dimensional Magnetic Bodies with Polygonal Cross-section. Geophysics, 37(3), 507–517. https://doi.org/10.1190/1.1440276.

[18] Ofoegbu, C. O. (1985). Curie point depths in Nigeria and their implications for geothermal exploration. *Geophysical Journal International, 80*(2), 391–408.

[19] Okubo, Y., Graf, R. J., Hansen, R. O., Ogawa, K., & Tsu, H. (1985). Curie point depths of the island of Kyushu and surrounding areas, Japan. *Geophysics, 50*(3), 481–494. https://doi.org/10.1190/1.1441926.

[20] Okubo, Y., & Matsunaga, T. (1994). Curie point depth in northeast Japan and its correlation with regional thermal structure and seismicity. *Journal of Geophysical Research, 99*(B11), 22363–22371. https://doi.org/10.1029/94JB01336.

[21] Pedersen, L. B. (1991). Relations between potential field anomalies and their gradient transformations. *Geophysics, 56*(6), 884–897. https://doi.org/10.1190/1.1443129.

[22] Reid, A. B., Allsop, J. M., Granser, H., Millett, A. J., & Somerton, I. W. (1990). Magnetic interpretation in three dimensions using Euler deconvolution. Geophysics, 55(1), 80–91. https://doi.org/10.1190/1.1442774.

[23] Salem, A., Williams, S., Fairhead, J. D., Smith, R., & Ravat, D. (2014). Interpretation of magnetic data using tilt-angle derivatives. *Geophysics, 79*(1), J1–J12. https://doi.org/10.1190/1.2799992.

[24] Shuey, R. T., Schellinger, D. K., Tripp, A. C., & Alley, L. B. (1977). Curie depth determination from aeromagnetic spectra. *Geophysical Journal International, 50*(1), 75–101. https://doi.org/10.1111/j.1365-246X.1977.tb01325.x.

[25] Silva, C. A., Bezerra, F. H. R., & Oliveira, L. F. S. (2006). Depth estimation using source parameter imaging of magnetic data. Journal of Applied Geophysics, 60(2), 133–144.

[26] Spector, A., & Grant, F. S. (1970). Statistical models for interpreting aeromagnetic data. *Geophysics, 35*(2), 293–302. https://doi.org/10.1190/1.1440092.

[27] Sebastian A S., Adetola S O., & Bello Y I. (2026). Geospatial and Aeromagnetic Investigation of Structural Lineaments in the Adamawa/Tarrasa region, Upper Benue Trough, NE Nigeria: An Implication for Geohazard Occurrence. *Nigerian Journal OF Physics NJP Volume 35(2)* .nipngr.org; https://doi.org/10.62292/njp.v35i2.2026.551.

[28] Tanaka, A., Okubo, Y., & Matsubayashi, O. (1999). Curie point depth based on spectrum analysis of magnetic anomaly data in East and Southeast Asia. *Tectonophysics, 306*(3–4), 461–470. https://doi.org/10.1016/S0040-1951(99)00072-4.

[29] Telford, W. M., Geldart, L. P., & Sheriff, R. E. (1998). *Applied geophysics* (2nd ed.). Cambridge University Press.

[30] Thurston, J.B, & Smith, R.S. (1997). Automatic conversion of magnetic data to depth, dip, and susceptibility contrast using the SPI (TM) method. Geophysics. 62(3):807–813. doi:10.1190/1.1444190.

[31] Ugwu, G. Z., & Alasi, T. K. (2016). Aeromagnetic survey for determining depth to magnetic source of Abakaliki and Ugep areas of the Lower Benue Trough, Nigeria. Engineering and Technology Journal, 1(1), 1–9.

[32] Yenne, E. Y., Green, C. M., & Torvela, T. (2025). Modelling geologic features and structures in the Middle and Lower Benue Trough of Nigeria from gravity and aeromagnetic data sets. Journal of African Earth Sciences, 231, 105745. https://doi.org/10.1016/j.jafrearsci.2025.105745.